Hindawi
Geofluids
Volume 2023, Article ID 9581827, 12 pages
https://doi.org/10.1155/2023/9581827

Research Article

Multipotential Surface Elastoplastic Constitutive Model and Its Application in the Analysis of the Phase II Cofferdam of the Three Gorges Project

Yong Wen,[1,2,3] **Guanghua Yang**,[4] **and Zhihui Zhong**[5]

[1]*College of Urban and Rural Construction, Zhongkai University of Agriculture and Engineering, Guangzhou 510225, China*
[2]*Guangdong Lingnan Township Green Building Industrialization Engineering Technology Research Center, Guangzhou 510225, China*
[3]*Institute of Sustainable Building and Energy Conservation of Zhongkai College of Agricultural Engineering, Guangzhou 510225, China*
[4]*Guangdong Research Institute of Water Resources and Hydropower, Guangzhou 510610, China*
[5]*Guangzhou Hongyu Design of Water Conservancy and Hydropower Co. Ltd., Guangzhou 511458, China*

Correspondence should be addressed to Yong Wen; wy876633@163.com

Received 20 April 2022; Revised 14 June 2022; Accepted 5 April 2023; Published 9 May 2023

Academic Editor: Di Feng

Based on multipotential surface theory, an elastoplastic constitutive model is established in this paper. The required parameters of the proposed model are the same as those of the Duncan-Chang model, and the proposed model is no longer restricted by the generalized form of Hooke's law. In addition, the proposed model uses a numerical method to fit the test curves to determine the required parameters. The calculation program of the proposed model is also developed by FLAC3D, and according to the comparison with the triaxial test results of gravel and the stress and deformation analysis of the phase II cofferdam of the Three Gorges Project, the rationality and superiority of the proposed model are verified.

1. Introduction

Among the existing constitutive models of soil, the Duncan-Chang model [1], which is based on the generalized form of Hooke's law, has been widely applied for simplicity in determining the required parameters, and all these parameters have a clear physical meaning. However, the largest issue with this model is that it does not reflect the dilatancy of soil. Although elastoplastic constitutive models [2–9] have some advantages over the Duncan-Chang model in reflecting the deformation characteristics of the soil, traditional elastoplastic constitutive models generally have to determine such as the plastic potential surface, yield function, and hardening rule. The determining processes are usually quite complicated and have more artificial assumptions; thus, the extent of their applications is less than that of the Duncan-Chang model. Therefore, it is of great significance to propose a model that can easily determine the parameters similar to the Duncan-Chang model and reflect the main deformation characteristics of soil, such as dilatancy.

To overcome the limitation of the traditional constitutive theory of soil, Yang et al. [10] proposed the multipotential surface theory (also known as generalized potential theory). This theory primarily uses a gradient vector of linearly independent multiple potential functions to express the stress-strain relationship of the main space. Then, the constitutive relation of the main space is transformed into a six-dimensional stress-strain relation by using the coordinate transformation method with a derivative, and the associated constitutive relation expressed by a potential function

is formed. This theory includes both the traditional elastic and plastic potential theories as its special cases and can express both the elastic and plastic constitutive relations; thus, it provides a new and more applicable theory for soil constitutive models [11, 12].

To develop the advantages of the Duncan-Chang model for parameter determination and to compensate for the theoretical limitation of generalized form of Hooke's law, an elastoplastic constitutive model based on multipotential surface theory is proposed in this paper. This multipotential surface elastoplastic constitutive model is no longer restricted by the generalized form of Hooke's law and can compensate for the inability of the Duncan-Chang model to reflect the dilatancy of soil. The proposed model is also applied to analyze the stress and deformation of the phase II cofferdam of the Three Gorges Project, and its rationality and superiority are then verified.

2. Multipotential Surface Elastoplastic Constitutive Model

Based on the multipotential surface theory, the establishment of the constitutive model is divided into two parts.

The first part is the establishment of the constitutive model in the principal space. Taking the principle stress space as the example, according to the test results, the constitutive model can be obtained as

$$\{\varepsilon_i\}_{3\times1} = [C]_{3\times3}\{\sigma_i\}_{3\times1}, \tag{1}$$

where $\{\varepsilon_i\}$ and $\{\sigma_i\}$ are the strain components and the stress components in the principal space, respectively, and $[C]$ is a 3×3 order matrix.

From a mathematical view, $\vec{\varepsilon} = (\varepsilon_1, \varepsilon_2, \varepsilon_3)$ can be seen as a three-dimensional vector and can be expressed by three potential functions with linearly independent gradient vectors $\phi_k (k = 1, 2, 3)$; then,

$$\varepsilon_i = \sum_{k=1}^{3} \lambda_k \frac{\partial \varphi_k}{\partial \sigma_i}, \tag{2}$$

where $\lambda_k (k = 1, 2, 3)$ are three undetermined coefficients, which can be determined by the test results in principal space.

The second part is the transformation from the constitutive model in principal space to the constitutive model in six-dimensional space. In the multipotential surface theory, this transformation is expressed by the derivative form, that is,

$$\varepsilon_{ij} = \sum_{m=1}^{3} \varepsilon_m \cdot \frac{\partial \varepsilon_m}{\partial \varepsilon_{ij}}. \tag{3}$$

Assuming that the principal strain $\{\varepsilon_m\}$ and the principal stress $\{\sigma_m\}$ are in the same direction, the following equation can be obtained:

$$\varepsilon_{ij} = \sum_{m=1}^{3} \varepsilon_m \cdot \frac{\partial \sigma_m}{\partial \sigma_{ij}}. \tag{4}$$

Substituting Equation (2) into Equation (4), then

$$\varepsilon_{ij} = \sum_{k=1}^{3} \lambda_k \cdot \frac{\partial \phi_k}{\partial \sigma_{ij}}. \tag{5}$$

Equation (5) is one of the full variable forms of the constitutive model based on the multipotential surface theory. Certainly, the incremental form of the constitutive model can also be obtained in the same way. For example, the constitutive model in principal stress space is obtained as

$$\{d\varepsilon_i^p\}_{3\times1} = [C]_{3\times3}\{d\sigma_i\}_{3\times1}, \tag{6}$$

where $\{d\varepsilon_i^p\}$ and $\{d\sigma_i\}$ are the plastic strain increment components and the stress increment components in principal space, respectively.

Similar to the above method, the following equation can be obtained:

$$\mathrm{d}\varepsilon_{ij}^p = \sum_{k=1}^{3} \mathrm{d}\lambda_k \frac{\partial \varphi_k}{\partial \sigma_{ij}}. \tag{7}$$

Equation (7) is one of the incremental forms of the constitutive model based on the multipotential surface theory. However, if the model is obtained based on the traditional plastic potential theory, then

$$\mathrm{d}\varepsilon_{ij}^p = \mathrm{d}\lambda \frac{\partial \varphi}{\partial \sigma_{ij}}. \tag{8}$$

Therefore, the traditional plastic potential theory can be seen as a special case of the multipotential surface theory.

Multipotential surface theory provides a new approach to the study of constitutive models of soil. The following is a simplified constitutive model of soil based on the multipotential surface theory.

In p-q space, when the influence caused by the rotation of the Lode angle and principal stress axes is neglected, the relationship between the plastic strain increment and stress increment can be written as

$$\left.\begin{aligned} \mathrm{d}\varepsilon_v^p &= A\mathrm{d}p + B\mathrm{d}q, \\ \mathrm{d}\bar{\varepsilon}^p &= C\mathrm{d}p + D\mathrm{d}q, \end{aligned}\right\} \tag{9}$$

where A, B, C, and D are called plasticity coefficients.

The total strain is the sum of the elastic strain and plastic strain, that is,

$$\left.\begin{aligned} \mathrm{d}\varepsilon_v &= \mathrm{d}\varepsilon_v^e + \mathrm{d}\varepsilon_v^p, \\ \mathrm{d}\bar{\varepsilon} &= \mathrm{d}\bar{\varepsilon}^e + \mathrm{d}\bar{\varepsilon}^p. \end{aligned}\right\} \tag{10}$$

According to the generalized form of Hooke's law and substituting Equation (9) into Equation (10), the following equation can be obtained:

$$\left.\begin{aligned} \mathrm{d}\varepsilon_v &= \left(A + \frac{1}{K_e}\right)\mathrm{d}p + B\mathrm{d}q, \\ \mathrm{d}\bar{\varepsilon} &= C\mathrm{d}p + \left(D + \frac{1}{3G_e}\right)\mathrm{d}q, \end{aligned}\right\} \tag{11}$$

where K_e is the elastic volume modulus and G_e is the elastic shear modulus.

According to the multipotential surface theory (Equation (7)), when $\phi_1 = p$ and $\phi_2 = q$, the following equation can be obtained:

$$\{\mathrm{d}\varepsilon^p\} = \lambda_1\left\{\frac{\partial p}{\partial \sigma}\right\} + \lambda_2\left\{\frac{\partial q}{\partial \sigma}\right\}, \tag{12}$$

where λ_1 and λ_2 are undetermined coefficients.

According to Equation (12), there is

$$\left.\begin{aligned} \lambda_1 &= \mathrm{d}\varepsilon_v^p, \\ \lambda_2 &= \mathrm{d}\bar{\varepsilon}^p. \end{aligned}\right\} \tag{13}$$

Substituting Equation (9) into Equation (13), the coefficients λ_1 and λ_2 can be written as follows:

$$\left.\begin{aligned} \lambda_1 &= A\mathrm{d}p + B\mathrm{d}q, \\ \lambda_2 &= C\mathrm{d}p + D\mathrm{d}q, \end{aligned}\right\} \tag{14}$$

while

$$\left.\begin{aligned} \mathrm{d}p &= \left\{\frac{\partial p}{\partial \sigma}\right\}^T\{\mathrm{d}\sigma\}, \\ \mathrm{d}q &= \left\{\frac{\partial q}{\partial \sigma}\right\}^T\{\mathrm{d}\sigma\}. \end{aligned}\right\} \tag{15}$$

Substituting Equation (14) and Equation (15) into Equation (12), the plastic strain can be obtained as

$$\{\mathrm{d}\varepsilon^p\} = \left[C_p^\sigma\right]\{\mathrm{d}\sigma\}, \tag{16}$$

where $[C_p^\sigma]$ is the plastic flexibility matrix and can be written as

$$\begin{aligned} \left[C_p^\sigma\right] = {} & A\left\{\frac{\partial p}{\partial \sigma}\right\}\left\{\frac{\partial p}{\partial \sigma}\right\}^T + B\left\{\frac{\partial p}{\partial \sigma}\right\}\left\{\frac{\partial q}{\partial \sigma}\right\}^T \\ & + C\left\{\frac{\partial q}{\partial \sigma}\right\}\left\{\frac{\partial p}{\partial \sigma}\right\}^T + D\left\{\frac{\partial q}{\partial \sigma}\right\}\left\{\frac{\partial q}{\partial \sigma}\right\}^T. \end{aligned} \tag{17}$$

Based on the elastic theory, the elastic strain can be obtained as

Table 1: Relation between the stress-strain and both E_t and μ_t.

	E_t and μ_t under different ε_1						
σ_3	0.5%		1.0%		1.5%		…
	E_t	μ_t	E_t	μ_t	E_t	μ_t	…

$$\{\mathrm{d}\varepsilon^e\} = [C_e^\sigma]\{\mathrm{d}\sigma\}, \tag{18}$$

where $[C_e^\sigma]$ is the elastic flexibility matrix.

Then, according to Equation (16) and Equation (18), the constitutive equation in the six-dimensional space can be obtained as

$$\{\mathrm{d}\varepsilon\} = \left(\left[C_e^\sigma\right] + \left[C_p^\sigma\right]\right)\{\mathrm{d}\sigma\}. \tag{19}$$

Equation (19) is called the simplified multipotential surface model, in which only four coefficients (A, B, C, and D) are needed.

3. Parameter Determination of the Multipotential Surface Elastoplastic Constitutive Model

3.1. Parameter Determination Based on the Duncan-Chang Model. Based on the previous analysis, to develop the simplicity of the Duncan-Chang model in determining the required parameters and compensate for its inability to reflect the dilatancy of soil, the multipotential elastoplastic model should be further established using the hyperbolic assumption of stress and strain in the Duncan-Chang model to determine the parameters.

According to the multipotential surface elastoplastic constitutive models, only the parameters of A, B, C, and D need to be determined. When the model satisfies the associated flow rule, the following equation can be obtained:

$$\begin{aligned} AD - BC &= 0, \\ B &= C. \end{aligned} \tag{20}$$

Thus, only two parameters need to be determined, which can be obtained by conventional triaxial compression tests. In the conventional triaxial compression tests, there is

$$\begin{aligned} \mathrm{d}p &= \frac{1}{3}\mathrm{d}\sigma_1, \\ \mathrm{d}q &= \mathrm{d}\sigma_1, \\ \mathrm{d}\varepsilon_v &= (1 - 2\mu_t)\mathrm{d}\varepsilon_1, \\ \mathrm{d}\bar{\varepsilon} &= \frac{2}{3}(1 + \mu_t)\mathrm{d}\varepsilon_1. \end{aligned} \tag{21}$$

Substituting Equation (21) into Equation (9), the following equation can then be obtained:

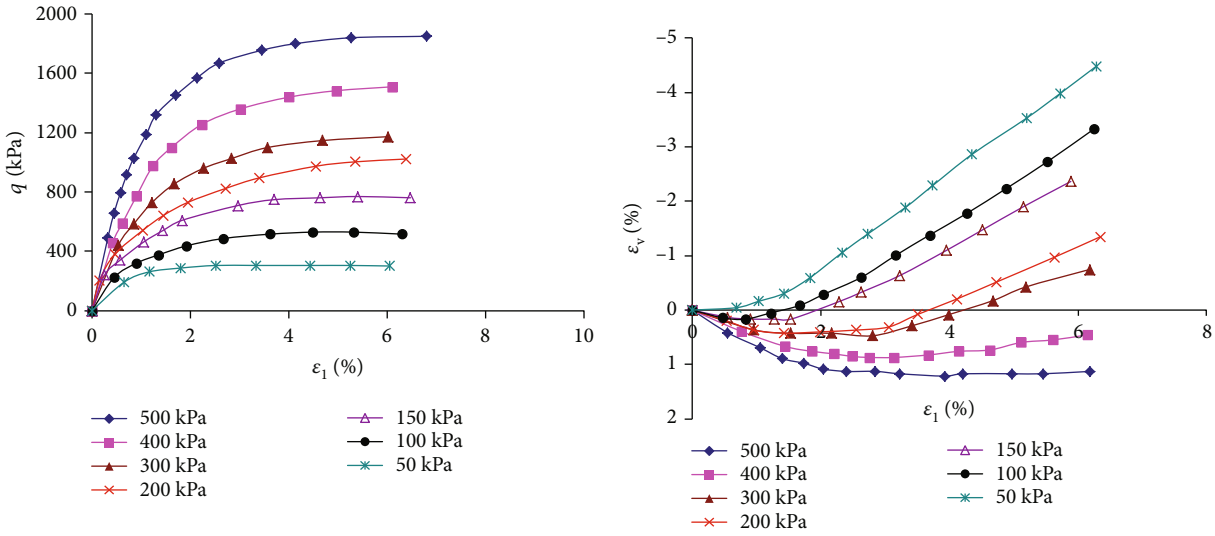

(a) Curves of the deviation stress and axial strain

(b) Curves of the volume strain and axial strain

Figure 1: Results of the triaxial tests of gravel (different confining pressures).

$$\begin{aligned}(1-2\mu_t)\frac{d\varepsilon_1}{d\sigma_1} &= \frac{1}{3}\left(A+\frac{1}{K_e}\right)+B,\\ \frac{2}{3}(1+\mu_t)\frac{d\varepsilon_1}{d\sigma_1} &= \frac{1}{3}C+\left(D+\frac{1}{3G_e}\right),\end{aligned} \tag{22}$$

where K_e is the bulk modulus ($=E_e/[3(1-2\mu)]$); G_e is the shear modulus ($=E_e/[2(1+\mu)]$); E_e and μ are the elastic modulus and Poisson's ratio, respectively, when unloading; and μ_t is the tangent Poisson's ratio, which can be determined by the hyperbolic assumption in the Duncan-Chang model.

$$\begin{aligned}\mu_t &= \frac{g-f\lg(\sigma_3/p_a)}{\{1-((d(\sigma_1-\sigma_3))/(Kp_a(\sigma_3/p_a)^n a))s\}^2},\\ a &= 1-R_f\frac{(\sigma_1-\sigma_3)(1-\sin\varphi)}{2c\cos\varphi+2\sigma_3\sin\varphi},\end{aligned} \tag{23}$$

where p is atmospheric pressure; σ_1 and σ_3 are the first and third principal stresses, respectively; and c, φ, K, n, R_f, d, g, and f are the soil material parameters that can be determined by the conventional triaxial test. Furthermore, the tangent modulus E_t is defined with $E_t=d\sigma_1/d\varepsilon_1$ and can also be determined by conventional triaxial tests.

$$\begin{aligned}\frac{1-2\mu_t}{E_t} &= \frac{1}{3}\left(A+\frac{1}{K_e}\right)+B,\\ \frac{2(1+\mu_t)}{3E_t} &= \frac{1}{3}C+\left(D+\frac{1}{3G_e}\right),\end{aligned} \tag{24}$$

where E_t is the tangent modulus that is determined according to the hyperbolic assumptions of stress and strain in the Duncan-Chang model.

$$E_t = Kp_a\left(\frac{\sigma_3}{p_a}\right)^n a^2, \tag{25}$$

$$a = 1-R_f\frac{(\sigma_1-\sigma_3)(1-\sin\varphi)}{2c\cos\varphi+2\sigma_3\sin\varphi}. \tag{26}$$

According to Equation (20) and Equation (24), the coefficients A, B, C, and D can then be obtained.

$$\begin{aligned}A &= \frac{K_{ep}^2}{G_{ep}+(1/3)K_{ep}},\\ B=C &= \frac{K_{ep}G_{ep}}{G_{ep}+(1/3)K_{ep}} = K_{ep}-\frac{1}{3}A,\\ D &= \frac{G_{ep}^2}{G_{ep}+(1/3)K_{ep}} = G_{ep}-\frac{1}{3}B,\end{aligned} \tag{27}$$

where

$$\begin{aligned}K_{ep} &= \frac{1-2\mu_t}{E_t}-\frac{1}{3K_e},\\ G_{ep} &= \frac{2(1+\mu_t)}{3E_t}-\frac{1}{3G_e}.\end{aligned} \tag{28}$$

The required parameters of the multipotential surface elastoplastic constitutive model can be determined by the Duncan-Chang model parameters. In addition, with the use of multipotential surface theory, the E_t and μ_t values of the proposed model are no longer limited by the generalized form of Hooke's law. When μ_t is greater than 0.5, the corresponding calculations can also be performed and do not cause the singularity of the stiffness matrix, so that the proposed model has more extensive adaptability.

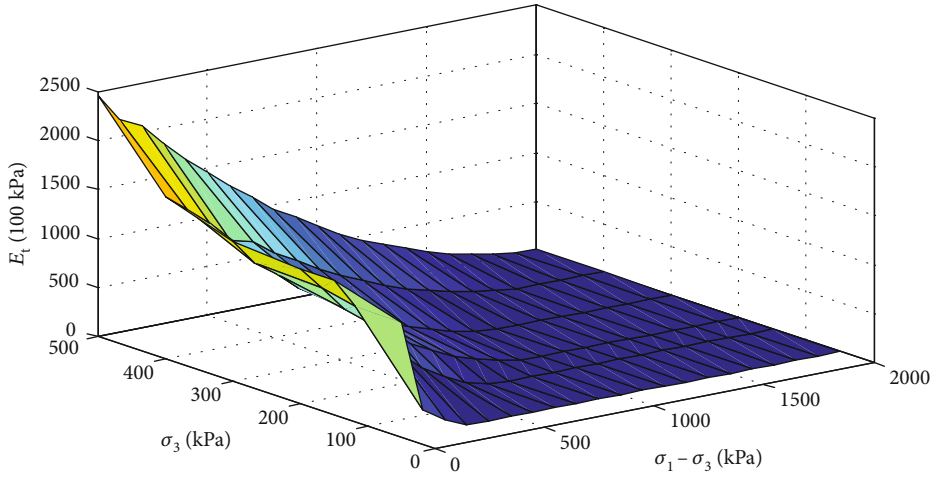

(a) Relationship of E_t with σ_3 and $\sigma_1 - \sigma_3$

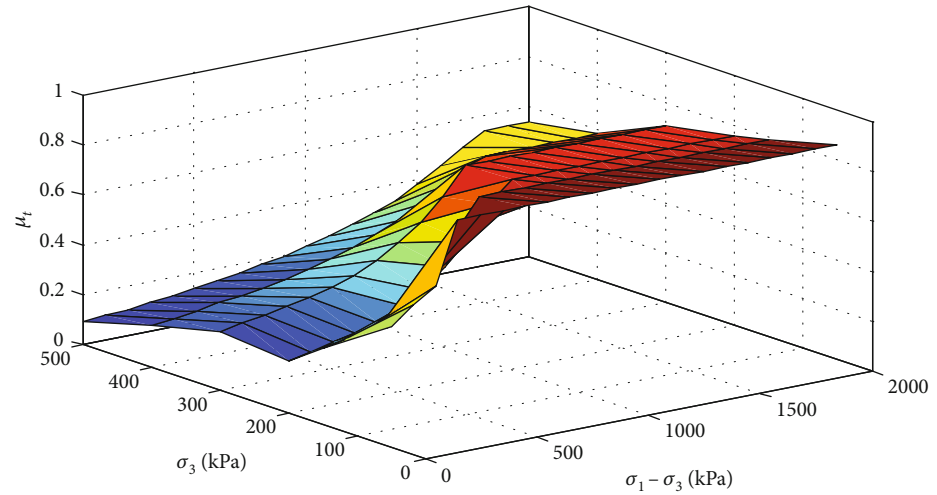

(b) Relationship of μ_t with σ_3 and $\sigma_1 - \sigma_3$

FIGURE 2: Parameters E_t and μ_t for the multipotential surface elastoplastic constitutive model.

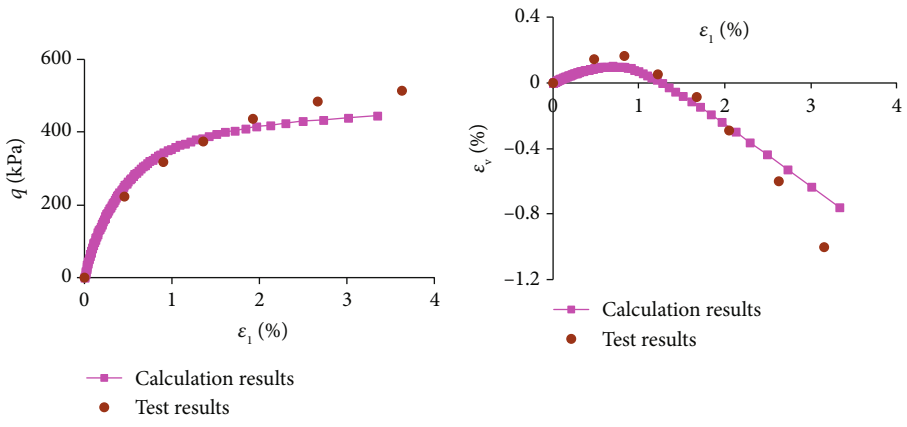

(a) Curves of the deviation stress and axial strain

(b) Curves of the volume strain and axial strain

FIGURE 3: Comparisons of calculation results of the multipotential surface elastoplastic constitutive model and test results ($\sigma_3 = 100$ kPa).

3.2. Determinations of the E_t and μ_t Values. The above section describes how to establish a multipotential surface elastoplastic constitutive model using the parameters of the Duncan-Chang model. Note that the E_t and μ_t values are still determined according to the hyperbolic assumptions used by the Duncan-Chang model, which has some

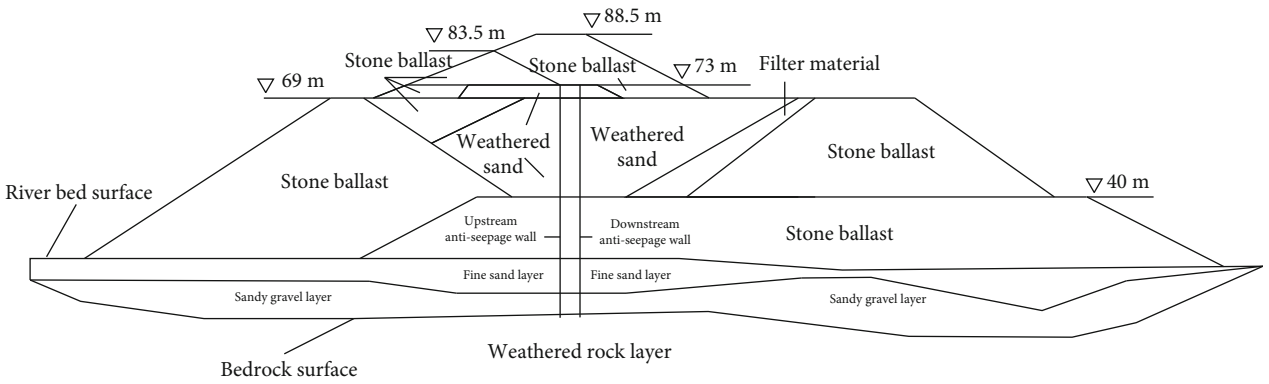

Figure 4: Profile schematic diagram of the phase II cofferdam of the Three Gorges Project.

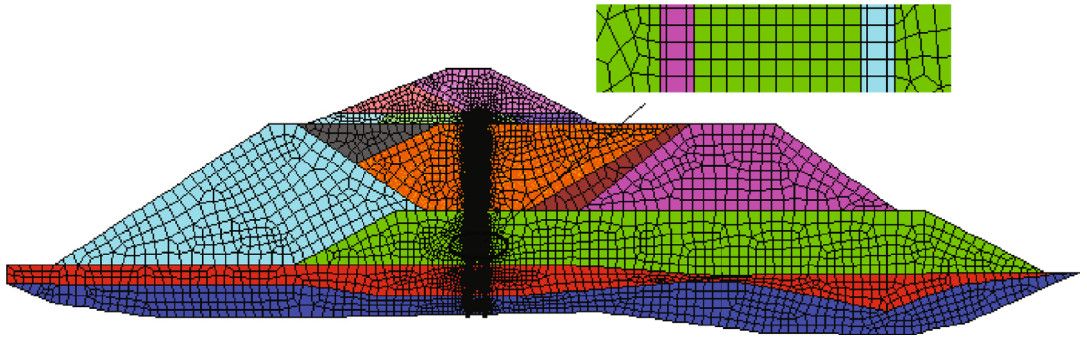

Figure 5: Numerical model and mesh divisions of the phase II cofferdam of the Three Gorges Project.

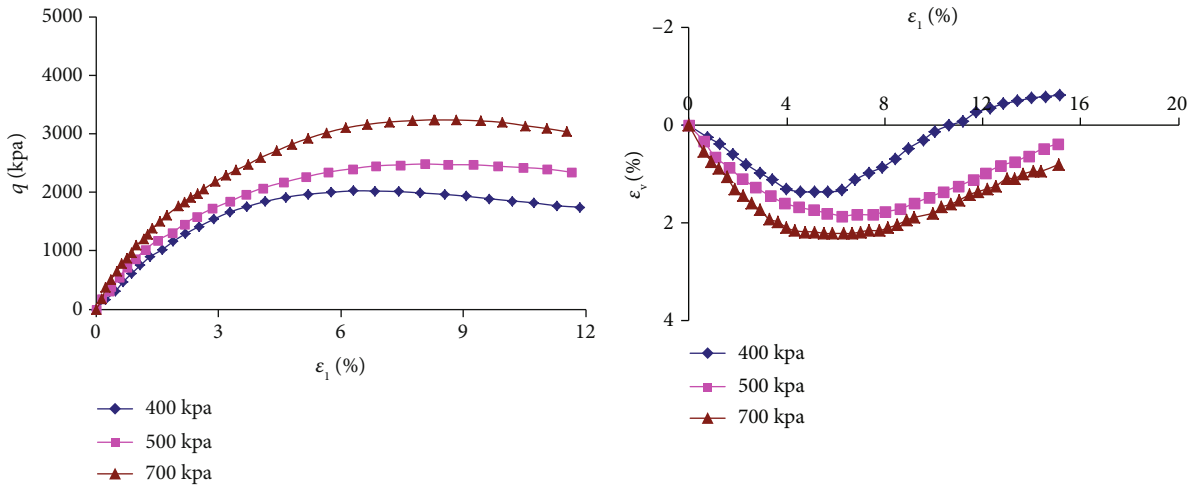

(a) Curves of the deviation stress and axial strain

(b) Curves of the volume strain and axial strain

Figure 6: Results of the triaxial tests of the stone ballast (different confining pressures).

limitations because some test curves do not necessarily conform to the hyperbolic function [13]. For example, for a test curve of the volumetric strain and axial strain with a dilatancy characteristic, the hyperbolic equation does not fit very well. For solving this problem, some scholars have modified the Duncan-Chang model, but due to the complexity of the nature of the soil, the empirical function always has some limitations. With the development of modern computer technology, the utilization of numerical methods is a worthwhile development direction. Therefore, on the basis of the multipotential surface elastoplastic constitutive model, this section further describes the use of numerical methods to determine the values of E_t and μ_t for this model.

In general, the results of conventional triaxial tests under different confining pressures can easily be fitted with functions, such as the least squares fitting method.

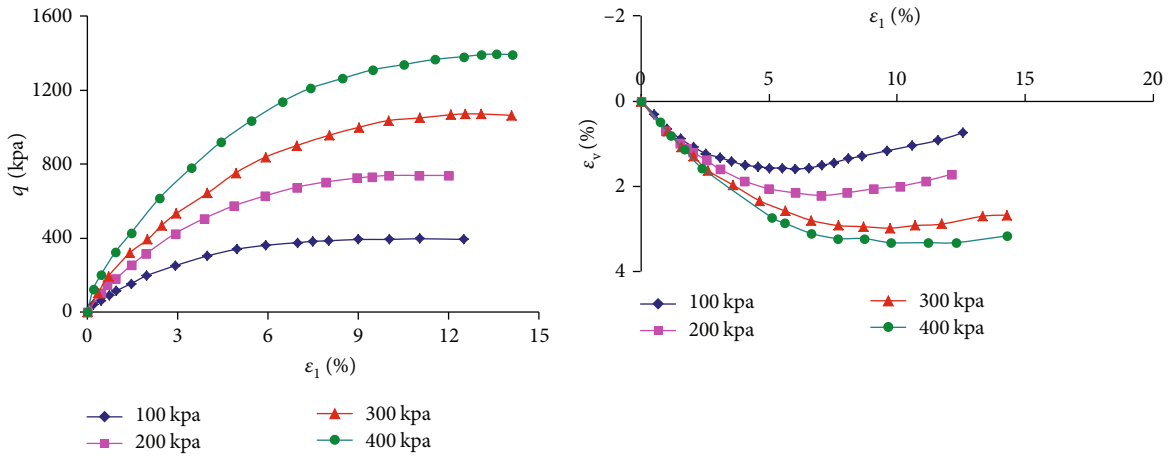

(a) Curves of the deviation stress and axial strain

(b) Curves of the volume strain and axial strain

Figure 7: Results of the triaxial tests of weathered sand (different confining pressures).

Table 2: Parameters of the Duncan-Chang model.

Materials	ρ (t/m^3)	φ (°)	c (t/m^2)	K	n	R_t	g	d	f
Stone ballast	1.99	38.5	10	650	0.34	0.8	0.37	2.70	0.30
Weathered sand	1.85	33.5	0	230	0.42	0.72	0.4	4.0	0.1
Filter material	1.95	38.5	0	500	0.73	0.86	0.40	4.30	0
Fine sand layer	1.84	37.0	2.0	420	0.44	0.80	0.30	7.90	0.15
Sandy gravel layer	2.23	40.0	0	800	0.4	0.8	0.36	1.45	0.15
Downstream antiseepage walls	2.15	34.3	128	12583	0.169	0.471	0.154	44.75	-0.427
Upstream antiseepage walls	2.15	34	178	12351	0.2864	0.336	0.2399	44.22	-0.105

Table 3: Parameters of the linear elastic model.

Materials	ρ (t/m^3)	E (MPa)	μ
Weathered rock layer	2.4	5000	0.25

The function expression based on fitting the test points is assumed as follows:

$$\begin{aligned} q &= f_1(\varepsilon_1, \sigma_3), \\ \varepsilon_v &= f_2(\varepsilon_1, \sigma_3), \end{aligned} \tag{29}$$

where f_1 and f_2 represent different function expressions.

For the conventional triaxial test, it can be deduced that $\sigma_3 = \text{Const}$. Thus, the following equations can be drawn:

$$E_t = \frac{\partial(\sigma_1 - \sigma_3)}{\partial\varepsilon_1} = \frac{\partial\sigma_1}{\partial\varepsilon_1}, \tag{30}$$

$$\mu_t = -\frac{d\varepsilon_3}{d\varepsilon_1}, \tag{31}$$

$$d\varepsilon_2 = d\varepsilon_3 = -\mu_t d\varepsilon_1, \tag{32}$$

$$d\varepsilon_v = d\varepsilon_1 + d\varepsilon_2 + d\varepsilon_3 = (1 - 2\mu_t)d\varepsilon_1, \tag{33}$$

$$\mu_t = \frac{1}{2}\left(1 - \frac{d\varepsilon_v}{d\varepsilon_1}\right), \tag{34}$$

where ε_2 and ε_3 are the second and the third main strain, respectively.

According to Equation (29), Equation (30), and Equation (34), the E_t and μ_t values can be obtained.

$$\begin{aligned} E_t &= \frac{\partial f_1}{\partial\varepsilon_1}, \\ \mu_t &= \frac{1}{2}\left(1 - \frac{\partial f_2}{\partial\varepsilon_1}\right). \end{aligned} \tag{35}$$

Generally, the results obtained from conventional triaxial tests cannot be too large due to the limitations in the number of confining groups. To make full use of the results of these test curves, the obtained E_t and μ_t values can be combined with the different points and constitute the database shown in Table 1.

In this way, for any point within the range of the stress-strain state in the above tables, the E_t values can be obtained by interpolation methods with adjacent points. For example, when using a binary cubic polynomial interpolation and assuming that $x = \sigma_3$ and $y = \varepsilon_1$, the expression of E_t is as follows:

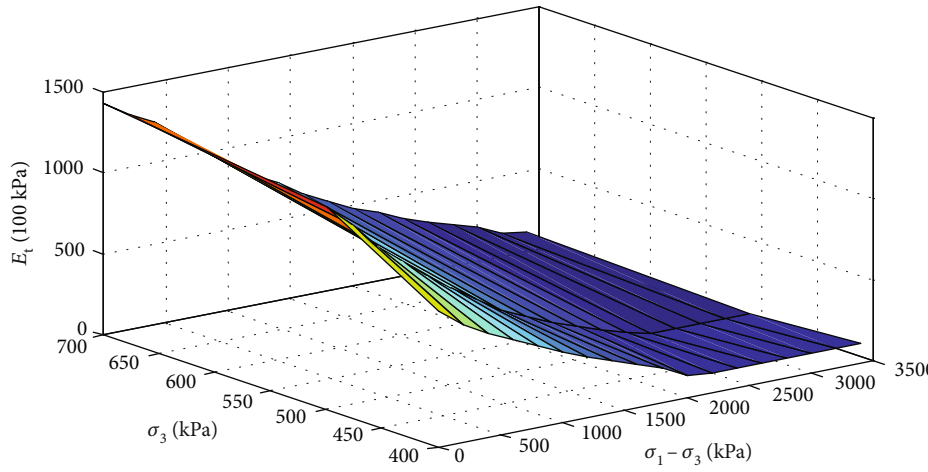

(a) Relationship of E_t with σ_3 and $\sigma_1 - \sigma_3$

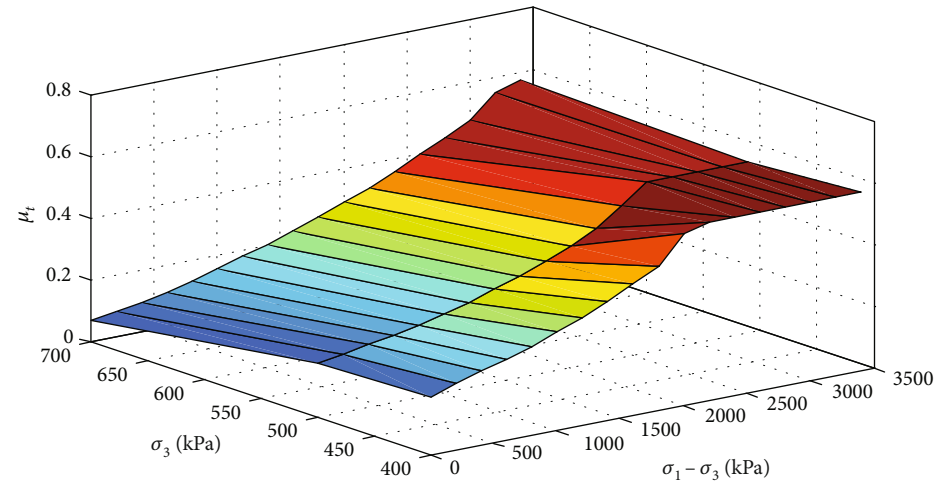

(b) Relationship of μ_t with σ_3 and $\sigma_1 - \sigma_3$

FIGURE 8: Parameters E_t and μ_t for the multipotential surface elastoplastic constitutive model (stone ballast).

$$E_t(x,y) = \sum_{r=i}^{i+2}\sum_{s=j}^{j+2}\left(\prod_{\substack{k=i\\k\neq r}}^{i+2}\frac{x-x_k}{x_r-x_k}\right)\left(\prod_{\substack{l=j\\l\neq s}}^{j+2}\frac{y-y_l}{y_s-y_l}\right)E_{trs}, \quad (36)$$

where E_{trs} is the function value at the point of (x_r, y_s).

Similarly, the μ_t values can also be determined by interpolation methods. Therefore, the multipotential surface elastoplastic constitutive model based on numerical methods is then obtained by the above method.

The above analysis indicates that the multipotential surface elastoplastic constitutive model not only develops the simplicity of the Duncan-Chang model in parameter determination but is also no longer limited by the generalized form of Hooke's law and can compensate for the inability of the Duncan-Chang model to reflect the dilatancy of soil. In addition, using the numerical method to fit the test curves can overcome the limitation of the Duncan-Chang model in which the hyperbolic function is used to determine the required parameters; thus, this proposed model has a wider range of adaptability.

4. Preliminary Verification of the Multipotential Surface Elastoplastic Constitutive Model

In this section, the multipotential surface elastoplastic constitutive model is preliminarily verified by taking the triaxial test result of gravel [14] under different confining pressures as an example. The triaxial test results are shown in Figure 1.

Based on the test results of confining pressures of 50 kPa, 150 kPa, 200 kPa, 300 kPa, 400 kPa, and 500 kPa, the results of confining pressures of 100 kPa can be predicted by the multipotential surface elastoplastic constitutive model. The model parameters E_t and μ_t can be obtained according to the numerical method introduced in Section 3.2, which can be expressed as Figure 2 (similar to Table 1). For any point in the stress state, E_t and μ_t can be obtained by the binary

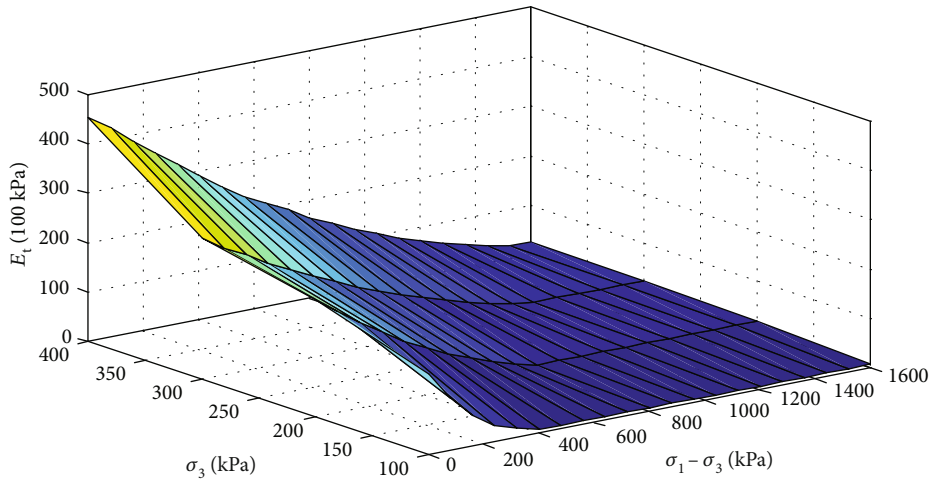

(a) Relationship of E_t with σ_3 and $\sigma_1 - \sigma_3$

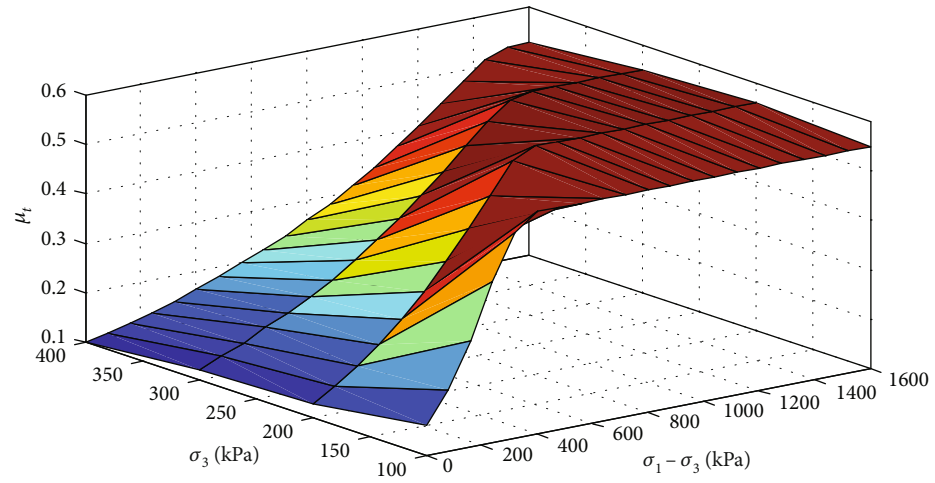

(b) Relationship of μ_t with σ_3 and $\sigma_1 - \sigma_3$

FIGURE 9: Parameters E_t and μ_t for the multipotential surface elastoplastic constitutive model (weathering sand).

cubic interpolation polynomial combined with the adjacent value points.

Figure 3 presents the comparisons of calculation results of the multipotential surface elastoplastic constitutive model and test results. The calculation results are similar to the test results, and the dilatancy of gravel is well reflected, which preliminarily verifies the rationality of the multipotential surface elastoplastic constitutive model.

5. Application of the Multipotential Surface Elastoplastic Constitutive Model

5.1. Profile of the Phase II Cofferdam of the Three Gorges Project. The phase II cofferdam of the Three Gorges Project consists of two cofferdams that are located in the upstream and downstream directions. The upstream cofferdam is 1440 m in length, has a maximum height of approximately 90 m, and is one of the most important and challenging buildings in the Three Gorges Project. This cofferdam is responsible for the protection of foundation pit excavation and the construction of power plants, and its stability and safety are directly related to the entire project. Therefore, the design and construction of the cofferdam are listed as one of the key technical problems of the Three Gorges Project. During the design process, the demonstration and calculation of different schemes were carried out for comparisons of the stress and deformation of the cofferdam and antiseepage walls. Finally, the plastic concrete low double row of antiseepage wall scheme of the cofferdam is adopted. The cofferdam is filled with stone ballast, weathered sand, and filter materials. The thickness of the two antiseepage walls is 1.0 m, and they are set into a weathered rock layer of approximately 1.0 m, and their center distance is approximately 6 m. The bottom of the cofferdam consists of a fine sand layer, a sandy gravel layer, and a weathered rock layer, as shown in Figure 4.

The stability and safety of the cofferdam mainly depend on the antiseepage walls, while for the antiseepage walls, their stability and safety primarily rely on the stress and deformation of the wall. These results of antiseepage walls are important bases for the stability and safety assessment of the whole cofferdam. The numerical method can predict the stress and deformation of the antiseepage walls and then evaluate the

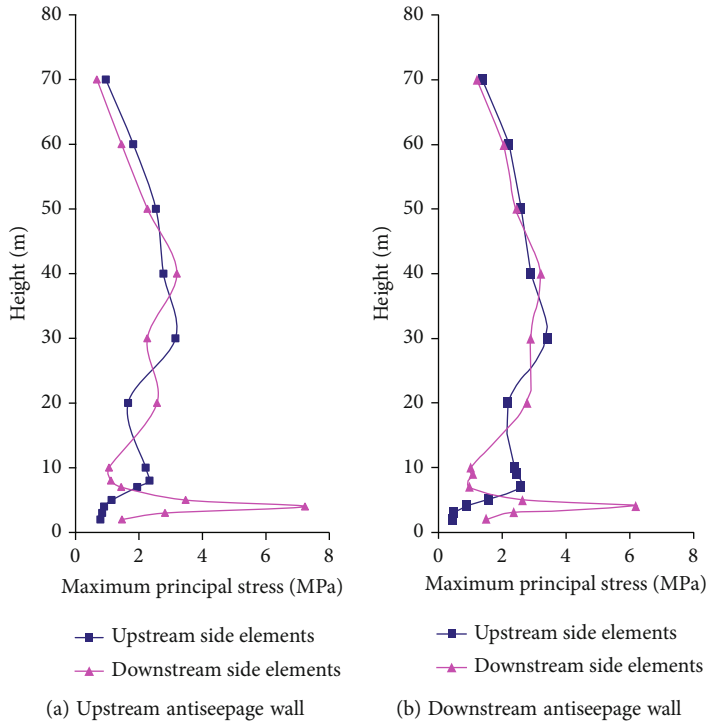

Figure 10: Calculation results of the maximum principal stresses by the Duncan-Chang model.

stability and safety of the antiseepage walls and cofferdam; thus, several associated investigations have been performed by some scholars, and the calculation results of various constitutive models, including nonlinear and elastoplastic, are then provided. Considering the dilatancy of the main fillers of cofferdams around the antiseepage walls (stone ballast and weathered sand), the multipotential surface elastoplastic model is adopted, and the stress and deformation of antiseepage walls and cofferdam are analyzed in this paper. The obtained results are also compared with the calculation results based on the Duncan-Chang model, and the rationality of the multipotential surface elastoplastic model is further verified.

5.2. Numerical Model and Parameters. The numerical software FLAC3D 3.00 is adopted, and the calculation program for the multipotential surface elastoplastic model is also developed. FLAC3D is a three-dimensional finite difference analysis software developed by Itasca Consulting Group, Inc., which has unique advantages in the fields of elastoplastic analysis, large deformation analysis, and construction process simulation of geotechnical materials. Figure 5 presents the numerical model and associated mesh divisions of the cofferdam. To better analyze the stress and deformation of the antiseepage walls, the antiseepage walls are divided into three rows of units with thicknesses of 0.2 m, 0.6 m, and 0.2 m.

Figures 6 and 7 provide the conventional triaxial test results of the main fillers. The test results show that both the stone ballast and weathered sand have a certain dilatancy. As the multipotential surface elastoplastic model has the advantage of reflecting the soil's dilatancy over the Duncan-Chang model, the required parameters can also be determined by conventional triaxial tests. Therefore, two numerical calculation schemes are carried out as follows: in the first scheme, the weathered rock layer is modeled by a linear elastic model, and the other materials are modeled by a Duncan-Chang model. In the second scheme, the weathered rock layer is still modeled by the linear elastic model, while the main fillers (the stone ballast and weathered sand) are modeled by the multipotential surface elastoplastic model, and the other materials are modeled by the Duncan-Chang model.

The parameters of the Duncan-Chang model and linear elastic model are provided according to references [15–17], as shown in Tables 2 and 3. The parameters of the multipotential surface elastoplastic model can be obtained according to the numerical method introduced in Section 3.2, which can be expressed as Figures 8 and 9. For any point in the stress state, E_t and μ_t can be obtained by the binary cubic interpolation polynomial combined with the adjacent value points.

5.3. Results and Discussion. The stability and safety of the cofferdam mainly depend on the antiseepage walls, while for the antiseepage walls, their stability and safety primarily rely on the stress and deformation of the walls. The antiseepage wall results are an important basis for the stability and safety assessment of the whole cofferdam. Therefore, the stress and deformation of antiseepage walls are thoroughly analyzed in this paper.

Figures 10 and 11 present the stress calculation results of both the upstream and downstream antiseepage walls under the worst condition in which the water levels of the upstream and foundation pits are separated by 85 m and

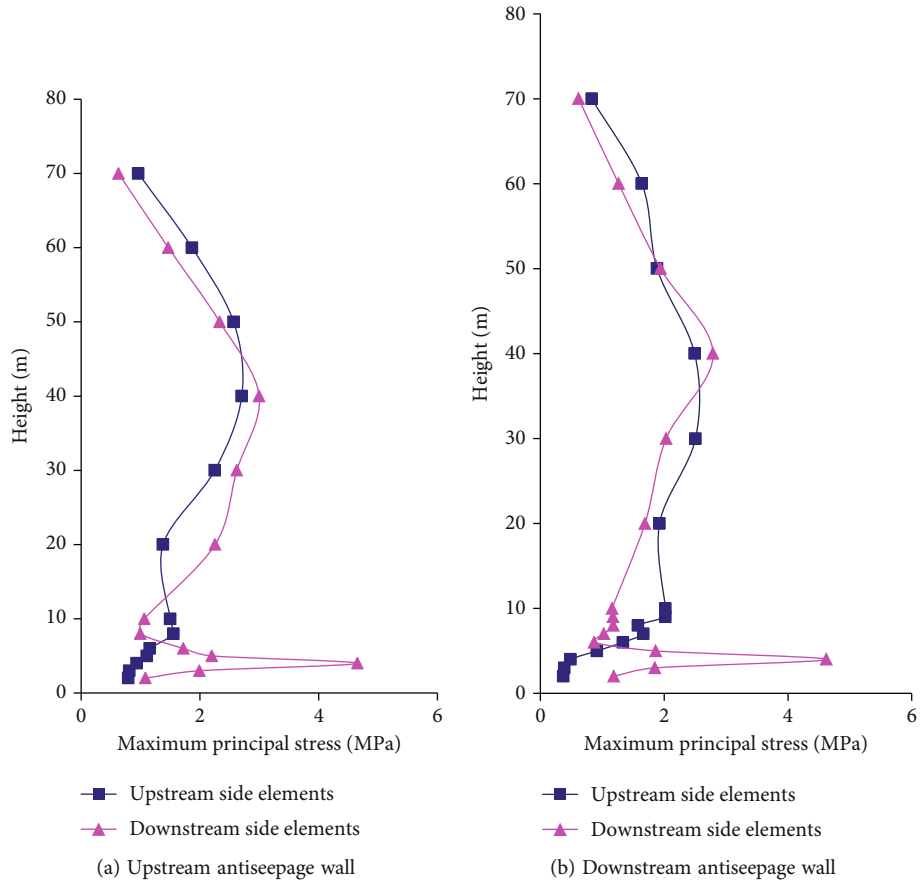

Figure 11: Calculation results of the maximum principal stresses by the multipotential surface elastoplastic model.

0 m, respectively. The maximum principal stress calculated by the Duncan-Chang model and the multipotential surface elastoplastic model both occur at the downstream side elements of the antiseepage walls near the bedrock surface. The maximum principal stresses of the upstream antiseepage wall are 7.2 MPa and 4.7 MPa, while those of the downstream antiseepage wall are 6.2 MPa and 4.6 MPa. It can be found that the maximum principal stresses calculated by the Duncan-Chang model are slightly larger than those based on the multipotential surface elastoplastic model. From the drilling sample test results, notably, the strength of the antiseepage wall is up to 4.62 MPa~11.2Mpa under unconfining pressure condition, which can be larger under confining pressure condition. This means that the stress results of the antiseepage walls calculated by the multipotential surface elastoplastic model are within the range of its strength, which agrees with the actual situation (the antiseepage walls are safe). While some individual element stress results of the antiseepage walls based on the Duncan-Chang model are beyond the range of its strength, this finding is not in agreement with the actual situation.

Figure 12 presents the deformation results of the upstream antiseepage wall calculated by the Duncan-Chang model and the multipotential surface elastoplastic model, which are also compared with the measured results. The calculation results of the multipotential surface elastoplastic model are superior to those based on the Duncan-Chang

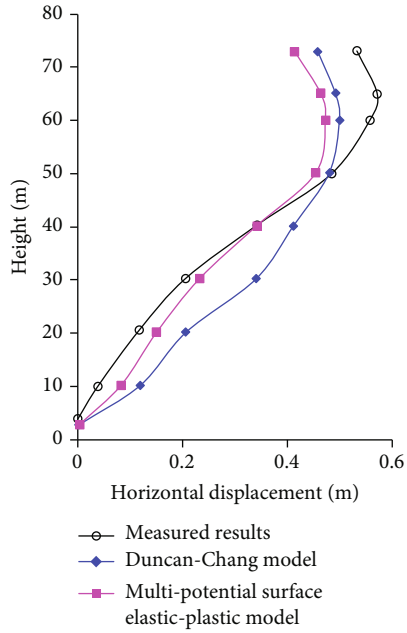

Figure 12: Comparisons between the calculation results and measured results of the horizontal displacement of upstream antiseepage wall.

model, especially for the deformation curvature and the value of the antiseepage wall near the bedrock surface, which is also the high stress level area. The stress calculation results mentioned above show that the maximum principal stresses based on the multipotential surface elastoplastic model are smaller than those based on the Duncan-Chang model and within the strength range of the antiseepage walls. The reasons can be noted from the deformation curvature and the value of the antiseepage wall near the bedrock surface; i.e., the deformation curvature and value based on the multipotential surface elastoplastic model are smaller than those of the Duncan-Chang model. Moreover, from Figure 12, the measured deformation curvature and value results of the antiseepage wall near the bedrock surface are even smaller than those of the multipotential surface elastoplastic model, which illustrates that the antiseepage walls are more secure. This observation can also be proven by the satisfactory operation of the antiseepage walls, which in turn verifies the rationality of the multipotential surface elastoplastic model.

6. Conclusions

The multipotential surface elastoplastic constitutive model proposed in this paper not only retains the simplicity of the Duncan-Chang model in parameter determination but is also no longer limited by the generalized form of Hooke's law and can compensate for the inability of the Duncan-Chang model to reflect the dilatancy of soil. Therefore, the proposed model is both for clay and sand. In addition, the multipotential surface elastoplastic constitutive model uses a numerical method to fit the test curves in determining the required parameters, which can overcome the limitation of the Duncan-Chang model in which the hyperbolic function is used. The rationality of the multipotential surface elastoplastic constitutive model is preliminary verified by comparisons with the triaxial test results of gravel with dilatancy. The application in the stress and deformation analysis of the phase II cofferdam of the Three Gorges Project further verifies the rationality and superiority of the multipotential surface elastoplastic model.

Data Availability

Some or all data, models, or code that support the findings of this study are available from the corresponding author upon reasonable request.

Conflicts of Interest

The authors declare that they have no conflicts of interest.

Acknowledgments

This research is supported by the Guangdong Basic and Applied Basic Research Foundation (no. 2020A1515110215) and National Natural Science Foundation of China (no. 52078143).

References

[1] J. M. Duncan and C. Y. Chang, "Nonlinear analysis of stress and strain in soils," *Journal of the Soil Mechanics and Foundations Division(ASCE)*, vol. 96, no. 5, pp. 1629–1653, 1970.

[2] J. B. Chen, "A monotonic bounding surface critical state model for clays," *Acta Geotechnica*, vol. 12, no. 1, pp. 225–230, 2017.

[3] W. X. Huang, J. L. Pu, and Y. J. Chen, "Hardening rule and yield function for soils," *Proceedings of the 10th International Conference on Soil Mechanic and Foundation Engineering*, 1981, pp. 631–634, Sweden, Stockholm, 1981.

[4] P. V. Lade and J. M. Duncan, "Elastoplastic stress-strain theory for cohesionless soil," *Journal of the Geotechnical Engineering Division(ASCE)*, vol. 101, no. 10, pp. 1037–1053, 1975.

[5] H. Matsuoka, Y. P. Yao, and D. A. Sun, "The Cam-Clay models revised by the _SMP_ criterion," *Soils and Foundations*, vol. 39, no. 1, pp. 81–95, 1999.

[6] C. Ma, D. C. Lu, X. L. Du, and A. N. Zhou, "Developing a 3D elastoplastic constitutive model for soils: a new approach based on characteristic stress," *Computers and Geotechnics*, vol. 86, pp. 129–140, 2017.

[7] K. H. Roscoe, A. N. Schofield, and A. Thurairajah, "Yielding of clays in states wetter than critical," *Géotechnique*, vol. 13, no. 3, pp. 211–240, 1963.

[8] Y. P. Yao, D. A. Sun, and H. Matsuoka, "A unified constitutive model for both clay and sand with hardening parameter independent on stress path," *Computers and Geotechnics*, vol. 35, no. 2, pp. 210–222, 2008.

[9] W. Zhang, J. Q. Zou, K. Bian, and Y. Wu, "Thermodynamic-based cross-scale model for structural soil with emphasis on bond dissolution," *Canadian Geotechnical Journal*, vol. 59, no. 1, pp. 1–11, 2022.

[10] G. H. Yang, G. X. Li, and Y. X. Jie, *The Multipotential Surface Theory of Soil Constitutive Model and Its Application*, China Water and Power Press, 2007.

[11] Y. M. Lai, Y. G. Yang, X. X. Chang, and S. G. Li, "Strength criterion and elastoplastic constitutive model of frozen silt in generalized plastic mechanics," *International Journal of Plasticity*, vol. 26, no. 10, pp. 1461–1484, 2010.

[12] A. Z. Zhou, T. H. Lu, and P. M. Jiang, "General description of soil-structure interface constitutive model based on generalized potential theory," *Rock and Soil Mechanics*, vol. 33, no. 9, pp. 2656–2662, 2012.

[13] T. Hyodo, Y. Wu, and M. Hyodo, "Influence of fines on the monotonic and cyclic shear behaviour of volcanic soil "Shirasu"," *Engineering Geology*, vol. 301, article 106591, 2022.

[14] H. Tian, *Experimental Study on Pile-Soil Interaction in Composite Foundation*, Tsinghua University, Department of Hydraulic Engineering, 1997.

[15] Z. L. Cheng, "Strain status of vertical impervious wall in TGP stage-2 upstream cofferdam," *Journal of Yangtze River Scientific Research Institute*, vol. 21, no. 6, pp. 34–38, 2004.

[16] M. Y. Wang, Z. L. Cheng, C. G. Bao, and Q. Y. Li, "Back analysis of the stage II cofferdam of the Three Gorges Project," *China Civil Engineering Journal*, vol. 40, no. 6, pp. 105–110, 2007.

[17] X. P. Zhang, C. G. Bao, and B. Shi, "Back analysis on the material parameters of the second stage cofferdam in the Three Gorges Project," *Chinese Journal of Rock Mechanics and Engineering*, vol. 20, no. 5, pp. 731–737, 2001.